JVI Journals.ASM.org

Neuroattenuation of Vesicular Stomatitis Virus through Picornaviral Internal Ribosome Entry Sites

Arun Ammayappan,[a] Rebecca Nace,[a] Kah-Whye Peng,[a] Stephen J. Russell[a,b]

Department of Molecular Medicine, Mayo Clinic, Rochester, Minnesota, USA[a]; Division of Hematology, Department of Medicine, Mayo Clinic, Rochester, Minnesota, USA[b]

Vesicular stomatitis virus (VSV) is potent and a highly promising agent for the treatment of cancer. However, translation of VSV oncolytic virotherapy into the clinic is being hindered by its inherent neurotoxicity. It has been demonstrated that selected picornaviral internal ribosome entry site (IRES) elements possess restricted activity in neuronal tissues. We therefore sought to determine whether the picornavirus IRES could be engineered into VSV to attenuate its neuropathogenicity. We have used IRES elements from human rhinovirus type 2 (HRV2) and foot-and-mouth disease virus (FMDV) to control the translation of the matrix gene (M), which plays a major role in VSV virulence. *In vitro* studies revealed slowed growth kinetics of IRES-controlled VSVs in most of the cell lines tested. However, *in vivo* studies explicitly demonstrated that IRES elements of HRV2 and FMDV severely attenuated the neurovirulence of VSV without perturbing its oncolytic potency.

Vesicular stomatitis virus (VSV), a member of the *Rhabdoviridae* family, replicates selectively in variety of cancer cells (1–5). VSV can infect a wide range of animals but primarily affects horses, donkeys, cattle, and swine. Human infection produces only influenza-like symptoms (6). VSV has a nonsegmented negative-strand RNA genome of approximately 11 kb encoding five structural proteins: nucleoprotein (N), phosphoprotein (P), matrix protein (M), glycoprotein (G), and RNA polymerase (L). The matrix (M) protein of VSV is multifunctional, aiding nucleocapsid packaging (7) and budding of the virion (8). It also shuts off host protein synthesis (9) and counteracts the host immune system (10).

Oncolytic virotherapy has shown considerable promise as an experimental approach to cancer therapy using replicating viruses for tumor destruction. Oncolytic viruses have been engineered or selected to exploit genetic defects in tumor cells (10, 11). Selective VSV replication in tumor cells has been attributed to their defective interferon (IFN) signaling compared with that of normal cells (4). Thus, VSV was shown to infect and kill the majority of the cancer cell lines in the NIH-60 panel, most of which had impaired responses to either IFN-α or IFN-β (4).

Although VSV is a promising oncolytic virus, its clinical translation has been long hindered by its notorious neuroinvasive properties. It causes neurotoxicity when administered by intranasal, intracranial, intravenous, and also intraperitonial routes (3, 12–14). Several strategies have been attempted to alleviate the neurotoxicity of VSV, such as mutation of the matrix protein (10), insertion of an interferon gene into the VSV genome (15), insertion of target sequences recognized by neuron-specific microRNAs (16), using semi-replication-competent vesicular stomatitis virus (17), and, finally, retargeting the virus by replacing its surface glycoprotein with other viral envelope proteins (18, 19). In this study, we used an alternative approach to control the neurotoxicity of VSV.

Translation of negative-sense RNA viruses depends on scanning by the ribosome from the 5′ end of the mRNA to the initiator AUG codon. In contrast, picornavirus RNAs do not depend on ribosomal scanning because they have an approximately 500-nucleotide (nt) highly structured internal ribosome entry site (IRES) at the 5′ end of the untranslated region (UTR), which mediates cap-independent RNA translation initiation (20–23). The exact molecular mechanism by which the host translation apparatus recognizes IRESs is still not clearly understood, but the process requires canonical translation initiation factors, as well as specific cellular proteins known as IRES *trans*-acting factors (ITAFs), which are normally not involved in cap-mediated initiation (24, 25).

In the case of foot-and-mouth disease virus (FMDV), the IRES element requires a specific factor, $ITAF_{45}$, for efficient translation. This factor is not expressed in murine brain cells, resulting in dramatic reduction of IRES-mediated translation in neuronal tissue (26). On the other hand, the activity of the human rhinovirus type 2 (HRV2) IRES is hindered by double-stranded RNA-binding protein 76 (DRBP76), which associates with the IRES in neuronal but not in malignant glioma cells. Thus, it was shown that depletion of DRBP76 from neuronal cells enhances rhinovirus IRES-driven translation and virus propagation (27). Placing essential viral genes under the control of an HRV2 IRES can attenuate the neurovirulence of poliovirus (28), herpesvirus (29), and rabies virus (30). We therefore sought to determine whether this neuron-selective inhibition of IRES elements could be exploited to control the expression level of vesicular stomatitis viral proteins in neurons, thereby ameliorating neurotoxicity.

MATERIALS AND METHODS

Cell culture. BHK, Vero, MPC-11, A375, HeLa, 293T, PC3, U87, Hep3B, and MDA MB-321 cells were obtained from American Type Culture Collection (ATCC), Manassas, VA, and were maintained in Dulbecco's modified Eagle's medium (DMEM) supplemented with 10% fetal bovine serum (FBS) in 5% CO_2. NB41A3 was purchased from ATCC and maintained in Ham's F-12 medium plus 3% FBS and 15% horse serum. HCN-2 primary human cortical neurons were purchased from ATCC, Manassas, VA, and cultured according to the manufacturer's instructions.

Received 22 October 2012 **Accepted** 27 December 2012
Published ahead of print 2 January 2013
Address correspondence to Stephen J. Russell, sjr@mayo.edu.

doi:10.1128/JVI.02984-12

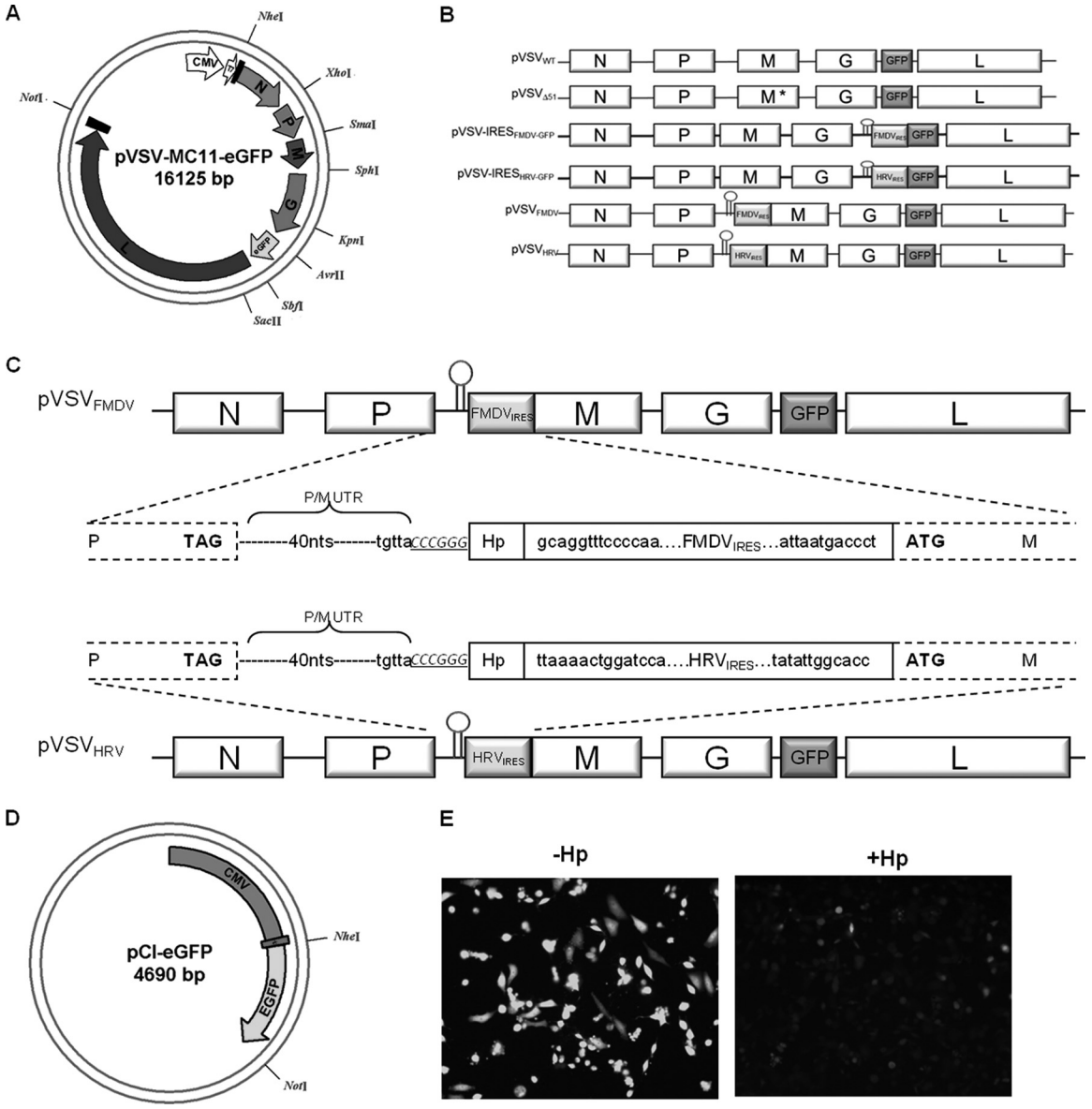

FIG 1 Construction and recovery of $pVSV_{IRES}$. (A) The circular map shows the structure of plasmid pVSV-MC11-eGFP with artificially inserted unique restriction sites. (B) A schematic representation of VSV genome constructs with IRES elements. The short hairpin is shown before the IRES at the 5′ end. M* indicates a matrix gene mutation (M51 deletion). (C) VSV genome constructs with FMDV and HRV IRES elements. The gene junction is shown in the middle. The $pVSV_{FMDV}$ and $pVSV_{HRV}$ plasmids were made by insertion of FMDV IRES and HRV IRES elements, respectively, before the start codon of the M gene (boxed). The hairpin is also shown (Hp). Capital bold letters are VSV P and M stop and start codons, respectively. The SmaI restriction site is shown in italics and underlined. The nucleotides (40 nt) between P and M ORF are shown as dotted lines (P/M UTR), and the last five nucleotides of the P/M gene junction are also shown (TGTTA). (D) The circular map shows the structure of plasmid pCI-eGFP, in which the eGFP ORF was inserted between NheI and NotI restriction sites. It was driven by the CMV promoter. A short hairpin (Hp) was inserted before the eGFP start codon. (E) Fluorescence microscopic images of BHK cells transfected with equal amounts of pCI-eGFP plasmid with or without hairpin.

KAS 6/1 multiple myeloma cells were a gift from Diane Jelinek (Mayo Clinic).

Plasmid construction and virus recovery. Plasmid DNA for VSV (pVSV-XN2), described previously (31), was used to construct a newly modified full-length VSV plasmid (pVSV-MC11) (Fig. 1A). The pVSV-MC11 was constructed in the pCI vector backbone (Promega Corp., Madison, WI). The VSV full-length genome was assembled between NheI and NotI restriction sites. Additional restriction sites were generated in the genome by mutational PCR. The enhanced green fluorescent protein (eGFP) open reading frame (ORF) was amplified from plasmid pIRES2-EGFP (Promega Corp., Madison, WI). A translation unit comprising the untranslated region (nucleotides between the stop codon of the G ORF and the start codon of the L ORF) between the G and L ORFs was fused at the C terminus of the eGFP ORF by PCR. New AvrII and SbfII restriction sites were introduced on either end of the modified eGFP ORF. The KpnI-SacII fragment was excised from the full-length pVSV-MC11 construct by restriction enzyme digestion and replaced with the modified KpnI-SacII fragment containing the eGFP gene, which creates pVSV-MC11-eGFP (Fig. 1A). The IRES element from foot-and-mouth disease virus was obtained by PCR amplification of plasmid pVITRO2 (Invivogen, San Diego, CA), and that from human rhinovirus 2 was obtained by custom gene synthesis (Life Technologies, Grand Island, NY). In order to generate the

pVSV-IRES-GFP, we inserted IRES elements of FMDV and HRV before the GFP open reading frame (Fig. 1B). $pVSV_{FMD}$ and $pVSV_{HRV}$ were generated by insertion of IRES elements from FMDV and HRV2, respectively, before the start codon of the matrix gene by overlapping PCR (Fig. 1C). A short hairpin (GGGGCGCGTGGTGGCGGCGAATTCGCCGCC ACCACGCGCCCC) was introduced before the IRES to hinder the cap-dependent translation (Fig. 1D and E).

Recombinant VSVs (rVSVs) were generated as follows. BHK cells were plated at a density of 1×10^6 cells/well in 6-well plates. The cells were infected with vaccinia virus encoding T7 polymerase at a multiplicity of infection (MOI) of 10. After an hour, vaccinia virus was removed, and the cells were transfected with 1 μg $pVSV_{IRES}$, 0.5 μg pN, 0.4 μg pP, and 0.2 μg pL (N, P, and L plasmids were constructed in the pCI vector) using 6.25 μl of Lipofectamine LTX transfection reagent (Life Technologies, Grand Island, NY) according to the manufacturer's instructions. The cells were incubated for 6 h at 37°C, and then the medium was replaced with DMEM plus 5% FBS. After 48 h, culture medium was harvested, filtered twice through a 0.2-μm filter, and overlaid onto new BHK cells in a 6-well plate. Forty-eight hours later, the culture medium was harvested, subjected to low-speed centrifugation, and titrated on fresh BHK cells. When necessary the recombinant viruses were further passaged to amplify the viral titer. For virus titration, BHK cells were grown on 96-well plates and infected with serially diluted virus stocks. GFP expression was considered an indicator of infection. Fifty percent tissue culture infectious dose ($TCID_{50}$) values were determined by the Spearman-Karber equation (32). The identities of the recombinant viruses were verified by subjecting genomic RNA to reverse transcription-PCR (RT-PCR) and sequence analysis.

Growth curves. For one-step growth curves, BHK cells were incubated with rVSVs at an MOI of 10.0 for 1 h at 37°C. Following this incubation, supernatant was removed, the monolayer was washed, and fresh growth medium was added. Supernatant was collected at predetermined time points (2, 4, 6, 8, 10, and 12 h), and the cell pellets were washed with phosphate-buffered saline (PBS) and stored at −80°C. For multistep growth curves BHK cells were incubated with rVSV at an MOI of 0.01 for 1 h at 37°C. Following this incubation, supernatant was removed, the monolayer was washed, and fresh growth medium was added. Supernatant was collected at predetermined time points (6, 12, 18, 24, 30, and 36 h), and the cell pellets were washed with PBS and stored at −80°C. Virus titer was determined by the $TCID_{50}$ method.

Western blot analysis. To detect viral protein expression levels, VSV-infected cells were harvested at the indicated time points and incubated with 100 μl of radioimmunoprecipitation assay (RIPA) buffer (25 mM Tris-HCl [pH 7.6], 150 mM NaCl, 1% NP-40, 1% sodium deoxycholate, 0.1% SDS) at 4°C for 10 min. The cell lysate was centrifuged, and the supernatant was collected and stored at −20°C until used. For immunoblotting, the proteins were electrophoretically separated in a 12% sodium dodecyl sulfate-polyacrylamide gel. VSV proteins were detected by Western blotting using polyclonal antibody against wild-type VSV (VSV_{wt}). We used ImageJ software (http://rsbweb.nih.gov/ij/) to quantify the bands obtained through immunoblotting.

***In vivo* experiments.** All animal protocols were reviewed and approved by the Mayo Clinic Institutional Care and Use Committee. BALB/c mice (female, 4 to 6 weeks old) were purchased from Jackson Laboratories. Mice were implanted with 5×10^6 mouse plasmacytoma (MPC-11) cells in the right flank. When tumors reached an average size of 0.2 to 0.5 cm^3 (day 9), mice were treated by single intravenous injection of rVSV. Tumor volume was measured using a hand-held caliper. For intracranial administration, rVSVs were administered in 30 μl of Opti-MEM carrier.

RNA extraction and quantitative RT-PCR. BHK cells were seeded in 6-well plates and infected with rVSVs at an MOI of 1.0. At the indicated time points, the supernatant was removed, and cells were washed with PBS. The cells were lysed in 400 μl RLT buffer (Qiagen, Valencia, CA), and total RNA was then extracted using the Qiagen RNeasy kit following the manufacturer's instructions. Quantitative two-step RT-PCR was performed according to the manufacturer's instructions (LightCycler 480 real-time PCR system; Roche Applied Science, Indianapolis, IN). For reverse transcription, a random hexamer was used, and this was followed by quantitative real-time PCR using primers directed against the N and M genes. In parallel, reverse transcription-quantitative PCR (RT-qPCR) directed against the glyceraldehyde 3-phosphate dehydrogenase (GAPDH) mRNA was performed to control the differences in the amounts of total input RNA. The relative copy number of target RNA was calculated from the ΔC_T value between GAPDH mRNA and target RNA. Total RNA from tissues was extracted and analyzed as described above.

High-resolution tumor analysis. Tumors harvested at 24-h intervals were frozen in optimal cutting medium (OCT) for sectioning. Tumor sections were analyzed by immunofluorescence for VSV antigens using polyclonal rabbit anti-VSV generated in-house by the Mayo Clinic Viral Vector Production Laboratory, followed by Alexa-labeled anti-rabbit IgG secondary antibody (Life Technologies, Grand Island, NY), and for cellular nuclei using Hoechst 33342 (Life Technologies).

Statistical analyses. The GraphPad Prism 4.0 program (GraphPad Software, San Diego, CA) was used for data handling, analysis, and graphic representation. Survival curves were plotted according to the Kaplan-Meier method, and survival function across treatment groups was compared using log rank test analyses. In all cases, two-tailed *P* values that are not adjusted for multiple comparisons are provided.

RESULTS

Recovery and growth kinetics of IRES-controlled vesicular stomatitis viruses. Since the matrix protein of vesicular stomatitis virus induces apoptosis and counteracts the host immune system, we decided to control its expression level using the internal ribosome entry site (IRES) elements of FMDV and HRV2. First, we incorporated the IRES elements before the GFP ORF to examine the effect of the mere presence of IRES elements in the VSV genome on virus replication (Fig. 1B). We also included a short hairpin at the 5′ end of IRES elements to prevent cap-dependent translation. The hairpin effect was tested by using plain GFP-expressing plasmid which was driven by the cytomegalovirus (CMV) promoter. The hairpin structure was inserted at the 5′end of the GFP gene. Compared with control GFP plasmid, stem-loop-inserted plasmid expresses significantly less or no GFP (Fig. 1D). The IRES-containing recombinant viruses showed growth characteristics similar to those of the parental VSV_{wt} in both single and multistep growth curve analysis (Fig. 2A and B). These data demonstrate that the presence of IRES elements in the VSV genome does not cause any negative effect on the virus replication. Next, we incorporated the IRES elements upstream of the start codon of the matrix gene without replacing the P and M gene junctions (this creates VSV_{FMDV} and VSV_{HRV}); in this way, the genomic structure of VSV was maintained (Fig. 1C). The IRES-controlled viruses exhibit a typical cytopathic effect (CPE), comparable to that of wild-type virus. Figure 2C shows the cytopathic effects of the recombinant viruses 24 h postinfection (p.i.) at an MOI of 0.01. An earlier study suggested that expressing G protein on the surface of a virus-infected cell in the absence of functional M protein, or with a reduced level of M, promotes cell fusion (33). This phenomenon was observed mainly in BHK cells, as demonstrated earlier (34).

To examine the effect of IRES elements on virus gene transcription, BHK cells were infected with rVSVs at an MOI of 1.0, and after 16 h p.i., cell lysates were collected and total RNA was extracted. The N and M transcripts were quantitatively analyzed by RT-qPCR and compared with those of parental virus. The IRES

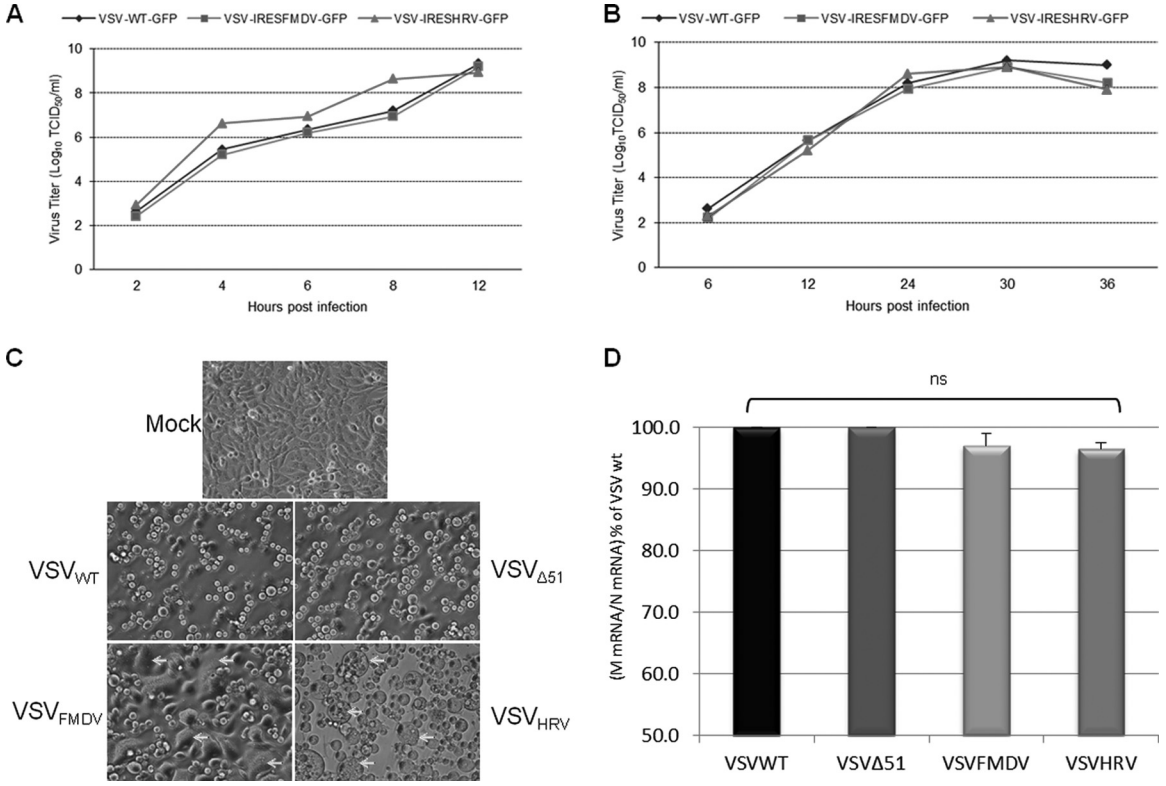

FIG 2 Analysis of growth properties of VSV carrying IRES elements. (A and B) Single-step (A) and multistep (B) growth curve analysis of the indicated viruses. (C) Phase-contrast microscopic images of BHK cells infected with VSV_{wt}, $VSV_{\Delta 51}$, VSV_{FMDV}, and VSV_{HRV} (24 h p.i. with an MOI of 0.01). Arrows indicate typical CPE produced by IRES viruses. (D) Relative expression of N and M genes from three replicates (16 h p.i. with an MOI of 1.0). Initially the VSV RNA levels were normalized to GAPDH RNA. The M/N mRNA ratio was determined and normalized to the VSV_{wt} M/N mRNA ratio and expressed as the mean percentage relative to VSV_{wt}. Error bars represent the standard error of the mean. Where error bars are not visible, the standard error was negligible.

elements had very little effect on VSV gene transcription. We observed no significant difference in M/N transcript ratios between parental and IRES-controlled viruses (Fig. 2D). This suggests that the presence of IRES elements affects significantly the translation and not the transcription of the M gene. To compare the replication kinetics of VSV_{FMDV}, VSV_{HRV}, VSV_{wt}, and also $VSV_{\Delta 51}$ (a matrix protein mutant) in detail, a multistep growth curve was performed by infecting BHK-21 cells at an MOI of 0.01 (Fig. 3A). VSV_{wt} and $rVSV_{\Delta 51}$ grew similarly, reaching approximately the same titer at the same time points. While VSV_{FMDV} grew slowly at initial time points, its titer at 36 h p.i. was similar to that of VSV_{wt}. In contrast, VSV_{HRV} grew very slowly, reaching a peak titer at 36 h p.i., which was ~2 logs lower than that of VSV_{wt}. Matrix protein expression was diminished in cells infected with either of the IRES-controlled viruses (Fig. 3A). We also performed one-step growth curves by infecting BHK-21 cells at an MOI of 10 to analyze a single cell cycle of viral replication (Fig. 3B). The growth pattern was comparable to that for multistep growth, but VSV_{HRV} reached a peak titer similar to that of VSV_{FMDV} and VSV_{wt}. These results demonstrate that IRES-controlled expression of matrix protein slows the kinetics of virus replication and can diminish virus yield.

IRES-dependent gene activity in a panel of cancer cell lines. To explore the cell-specific activity of IRES elements, we studied the growth characteristics of VSV_{FMDV} and VSV_{HRV} in various cancer cell lines. The virus titer and expression levels of M protein after 12 h p.i. with an MOI of 10.0 are shown in Fig. 4. The viral M protein was chosen as a target to be controlled in neuronal tissue because it plays a major role in virus virulence. IRES-mediated control of the M gene should not reduce the transcription and the translation of other viral genes but should specifically interfere with the matrix gene translation. The IRES elements of both FMDV and HRV2 function well in most of the cancer cell lines tested and at the same time cause a reduction in the titer of VSV_{FMDV} and VSV_{HRV} compared to that of VSV_{wt}. The neuronal cell lines 293T and U87 supported the growth of IRES-controlled VSVs (Fig. 4A). There was significant reduction in the virus titer (~3.5 logs) and M protein accumulation (VSV_{HRV}) in NB41A3 cells (neuroblastoma) compared to in other cell lines (Fig. 4B and C). The MDA MB-231 (breast cancer), HeLa (cervical cancer), and PC3 (prostate cancer) cells were relatively resistant to VSV infection (35). There was a 2-log reduction in the titer of VSV_{wt} in these cell lines, and VSV_{FMDV} and VSV_{HRV} grew a log lower than VSV_{wt}, which was associated with a marked to moderate reduction in M gene expression (Fig. 4A and B). There was significant reduction in M gene translation in case of multiple myeloma cell lines Kas 6/1 and MPC-11. In general, the translation efficiency of the HRV2 IRES is lower than that of the FMDV IRES in most of the cell lines tested. It was demonstrated that the ΔM51 mutant VSV ($VSV_{\Delta 51}$) is a potent inducer of interferon (10) and is highly sensitive to the host antiviral response. Its replication is therefore highly restricted in the interferon-responsive cell lines (NB41A3,

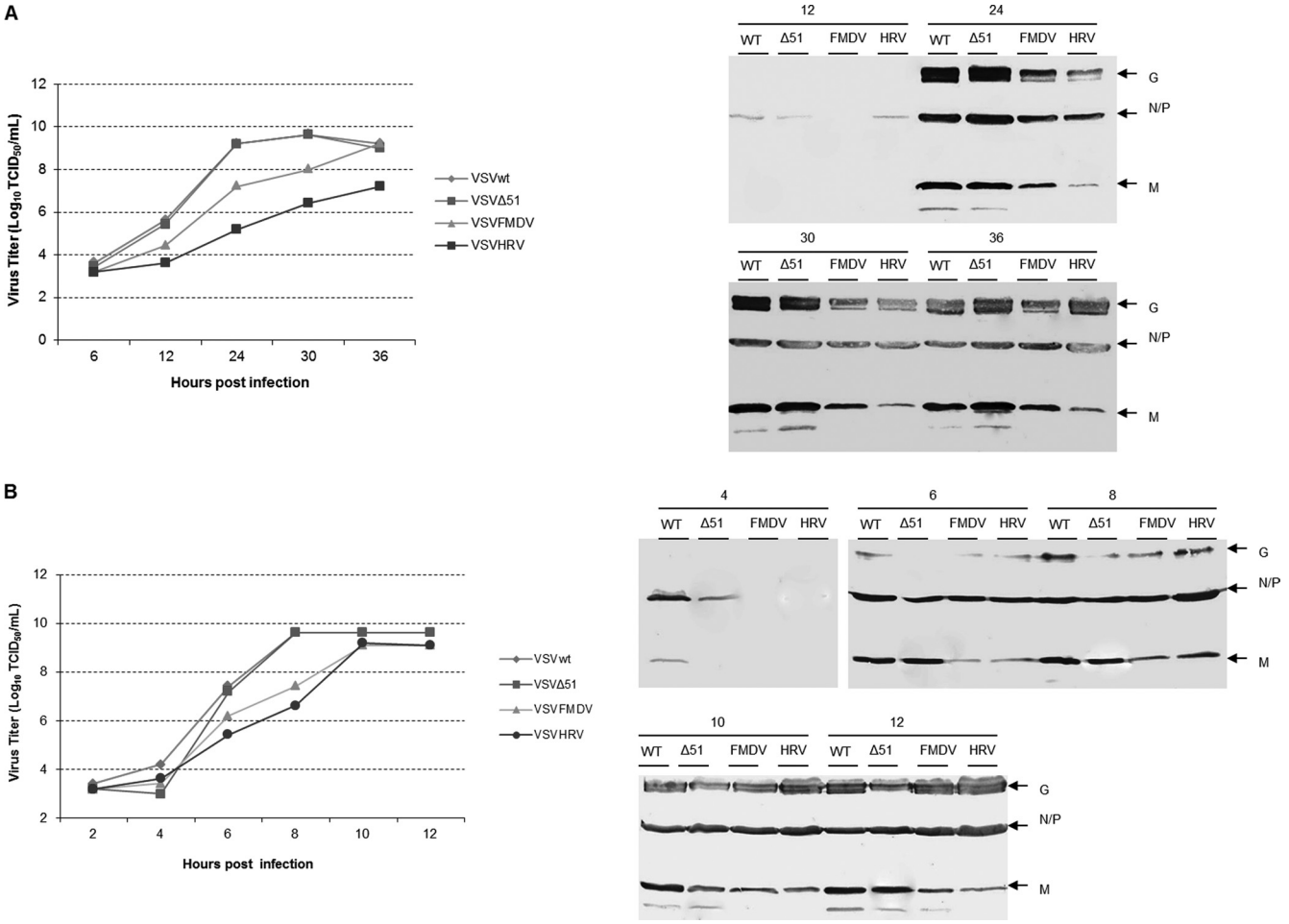

FIG 3 Analysis of viral growth kinetics. (A) Multistep growth curve. Replication of VSV_{wt}, $VSV_{\Delta 51}$, VSV_{FMDV}, and VSV_{HRV} in BHK cells at an MOI of 0.01 is shown. Supernatants were collected from infected cells at the indicated time points, and virus titers were calculated by standard $TCID_{50}$ assay. Cell lysates were harvested and analyzed for the virus-specific proteins by Western blotting. (B) Single-step growth curve. Replication of VSV_{wt}, $VSV_{\Delta 51}$, VSV_{FMDV}, and VSV_{HRV} in BHK cells at an MOI of 10.0 is shown. Supernatants were collected from infected cells at the indicated time points, and virus titers were calculated by standard $TCID_{50}$ assay. Cell lysates were harvested and analyzed for the VSV-specific proteins by Western blotting.

MDA MB-213, PC3, and HeLa). Overall, IRES-dependent translation of the matrix gene mRNA was less efficient than its cap-dependent translation, leading to a reduction in M protein gene expression in most of the cell lines tested.

Replication of IRES-controlled recombinant VSVs in primary neuronal cells. It was previously demonstrated that the IRES elements of HRV2 and FMDV attenuated the neurovirulence of poliovirus and Theiler's murine encephalomyelitis virus (TMEV), respectively, by impairing their ability to replicate in neuronal tissues (27, 36). Also, Marschalek et al. (30) suggested that HRV2 IRES insertion might provide a basis for the neuroattenuation of rabies virus. We therefore characterized the protein expression and growth properties of our IRES-controlled VSVs in primary human cortical neuronal cells (HCN-2) infected at an MOI of 10 (Fig. 5).

Forty-eight hours after infection with VSV, marked cytopathic effects were seen in the primary neuronal cells (Fig. 5A). Protein expression studies showed significant reduction in the M protein expression levels in cells infected with IRES-controlled viruses compared to those infected with VSV_{wt} (Fig. 5B). In contrast, N/P protein expression from IRES-controlled viruses was maintained at almost the same level as for VSV_{wt}. Both IRES elements were poorly functional in primary neuronal cells, resulting in an ~3-log reduction in viral titers (Fig. 5C). The $VSV_{\Delta 51}$ virus was unable to counteract the host innate immunity, and its replication was highly restricted in neuronal cells.

Evasion of interferon-mediated antiviral immunity. Vesicular stomatitis virus uses its matrix protein to avert the host innate immune response. The matrix protein has the ability to interrupt cellular transcription and also mRNA export from the nucleus, both of which function to antagonize the host immune response (37). Reducing the level of M protein in the cell may attenuate its ability to shut off host protein translation and to block the establishment of an IFN-mediated antiviral state but would not be expected to completely destroy this activity as with the ΔM51 mutation. To examine the immune evasion properties of IRES-controlled VSVs, HeLa cells were treated with human IFN-α at concentrations of 0, 1, and 50 U/ml and 24 h later were infected with rVSVs at an MOI of 1.0. Figure 6A to C show that there is significant reduction in virus-infected cells treated with 50 U/ml

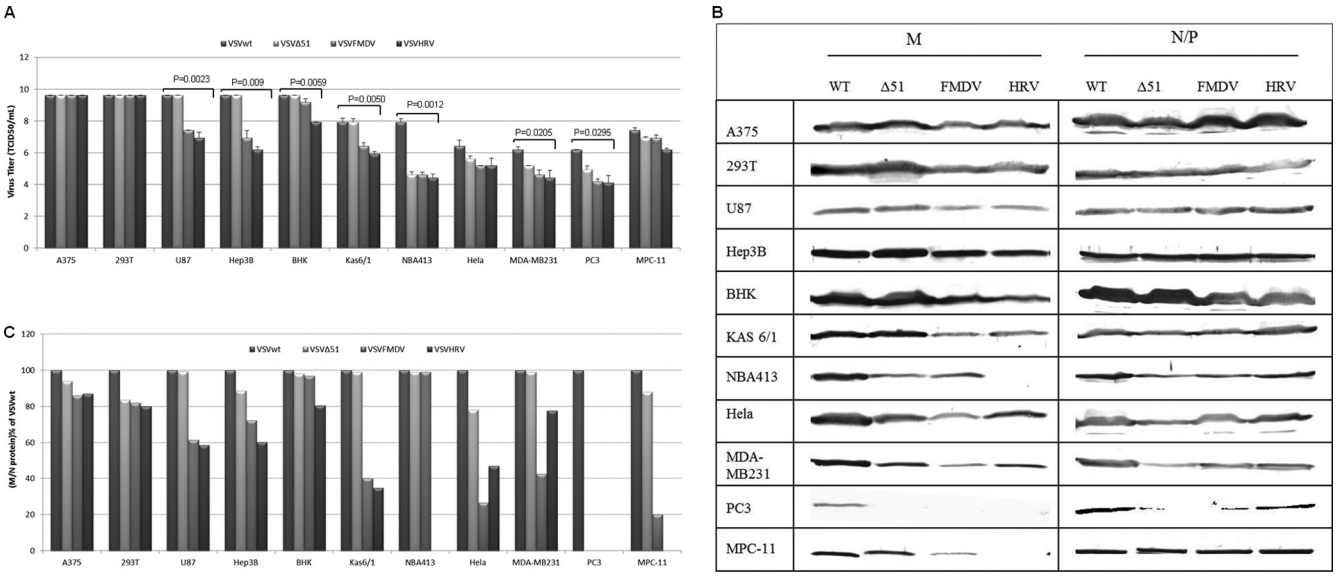

FIG 4 Growth properties of IRES-controlled viruses in various cancer cell lines. (A) After 12 h p.i. (MOI, 10.0), viral titers were determined by standard $TCID_{50}$ assay. Average titers and standard deviations (SDs) (error bars) for the three replicates are shown. (B) Cell lysates were harvested after 12 h p.i. and analyzed for the virus-specific proteins by Western blotting. (C) Initially, densitometry was performed using ImageJ software for the blots shown in panel B. The M/N-P protein ratio was determined, normalized to the VSV_{wt} M/N-P protein ratio, and expressed as the percentage relative to VSV_{wt}.

but, interestingly, that the titers of the IRES-controlled viruses are reduced only 10-fold, approximately the same as for VSV_{wt}. In contrast to the IRES-controlled viruses $VSV_{\Delta 51}$ is highly sensitive to the IFN-stimulated cellular antiviral response, which leads to a 100-fold reduction in viral titer. Thus, in contrast to the Δ51 M mutation, IRES-controlled translational attenuation of M does not appreciably limit the ability of the virus to counteract the cellular IFN response.

***In vivo* neuroattenuation of IRES-controlled VSVs.** Having characterized the growth properties of IRES-controlled VSVs in primary neurons and neuronal cell lines, we next proceeded to evaluate their toxicity profiles *in vivo*. Since VSV causes lethal encephalitis when inoculated directly into the brain, we started with a low-dose inoculum. Four- to 6-week-old BALB/c mice were inoculated intracranially with 1×10^4 $TCID_{50}$s of rVSVs and monitored closely for signs of neurotoxicity. No complications were seen in animals injected with only Opti-MEM. Wild-type VSV was highly lethal at this lowest dose, killing 80% of the mice within 7 days of injection (Fig. 7A). Euthanasia was typically done because of hind limb paralysis or other signs of neurotoxicity. All other virus-inoculated mice survived with no symptoms until the termination of the study (30 days). The survival advantage of mice inoculated with IRES-controlled VSVs was significant compared to survival of those inoculated with VSV_{wt} ($P = 0.0144$).

We next injected higher doses of the rVSVs, ranging from 10^6 to 10^8 $TCID_{50}$s, into the brains of 4- to 6-week-old BALB/c mice. VSV_{FMDV} caused no mortality at 10^6 $TCID_{50}$s, but at 10^7 $TCID_{50}$s it caused 60% mortality (Fig. 7B). Further analysis of infected brain tissues by immunostaining (Fig. 7C) and RT-qPCR (Fig. 7D) supports our observation. All mice inoculated with VSV_{HRV} survived without any neurotoxicity even at the highest dose level (10^8 $TCID_{50}$s), as did $VSV_{\Delta 51}$-infected mice. This study reveals that the HRV2 IRES renders the recombinant VSV completely apathogenic, whereas the FMDV IRES reduces the neurotoxicity significantly. Thus, as suggested earlier (30), neuroattenuation of the IRES-controlled VSVs *in vivo* was dependent on the degree of IRES translation initiation.

IRES-controlled recombinant VSVs retain their oncolytic efficacy *in vivo*. Since the ultimate goal of this study was to generate neuroattenuated oncolytic VSV, we next sought to determine whether the IRES-controlled viruses retain their oncolytic potency *in vivo*. Our *in vitro* studies (see above) show that, while they may have slower growth kinetics, the IRES-controlled VSVs can infect and kill various cancer cell types as effectively as the wild-type virus. Thus, the IRES elements of FMDV and HRV2 are highly functional in these cancer cell lines. Mouse plasmacytoma (MPC-11) cells and the subcutaneous tumors that grow after their subcutaneous implantation are highly susceptible to VSV infection. Four- to 6-week-old immunocompetent BALB/c mice were implanted with MPC-11 cells (5×10^6) subcutaneously. When tumors reached approximately 100 to 500 mm^3, the animals were treated with a single intravenous dose of 10^8 $TCID_{50}$s of rVSVs and were monitored daily for health status and tumor size.

Untreated control tumors grew quickly, and all animals in the virus treatment groups were euthanized by day 9 after initiation of therapy (when tumors reached ≥2,000 mm^3 or developed internal metastases) (Fig. 8A). Animals treated with $VSV_{\Delta 51}$ or IRES-controlled VSVs showed significant tumor regression (Fig. 8B to D) and prolonged survival (Fig. 8E and F) but eventually relapsed, necessitating euthanasia of all animals. None of the animals showed any sign of neurotoxicity. There was no significant difference in the antitumor efficacies of VSV_{FMDV} and VSV_{HRV} ($P > 0.05$). To confirm the virus replication in the tumor parenchyma, selected tumors were harvested at 24, 48, and 72 h after virus administration and subjected to immunofluorescence to detect VSV antigens. Figure 9A shows that the virus infection starts as foci at 24 h and spreads to the whole tumor as time progress. The spread of VSV_{HRV} was slower than that of VSV_{FMDV}. Quantitative

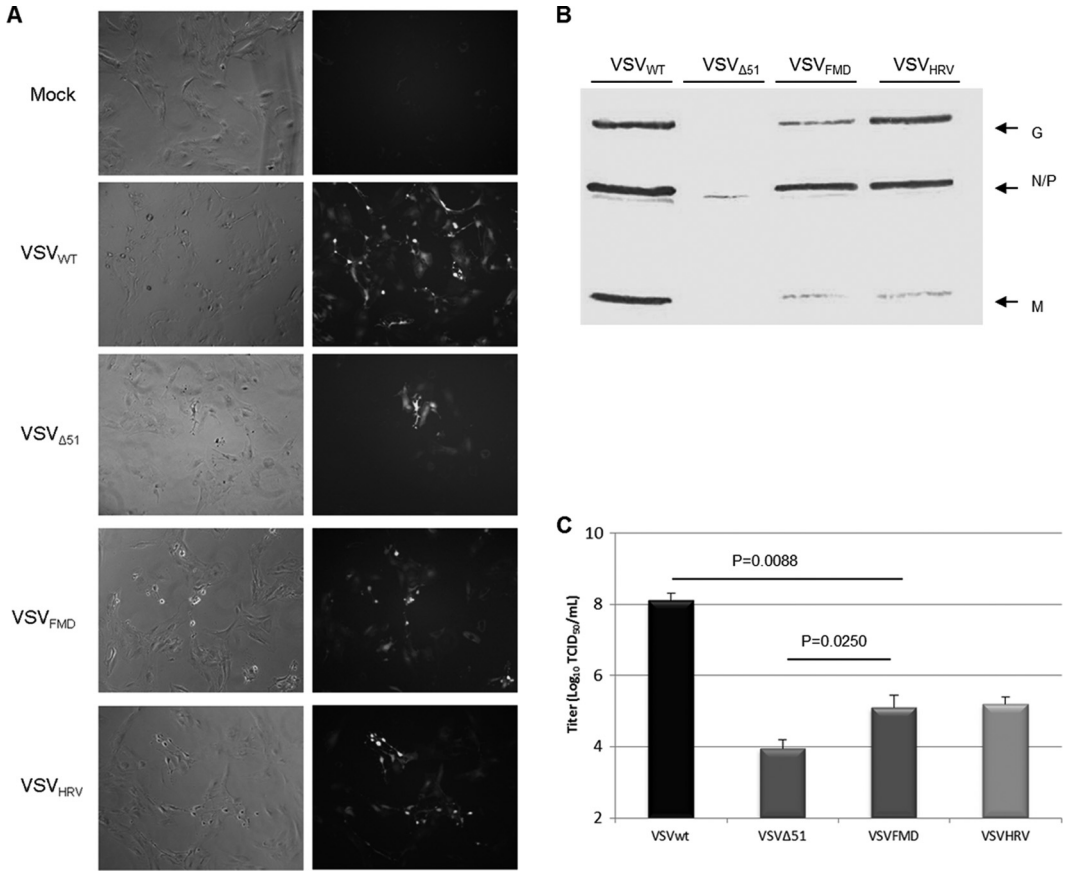

FIG 5 Growth properties of rVSVs in primary human neuronal cell. (A) Phase-contrast and fluorescence microscopic images of primary human cortical neuronal cells (HCN-2) infected with VSV$_{wt}$, VSV$_{\Delta 51}$, VSV$_{FMDV}$, and VSV$_{HRV}$ (48 h p.i. with an MOI of 10.0). (B) Cell lysates were harvested and analyzed for the virus-specific proteins by Western blotting. (C) Supernatants were collected from infected cells after 48 h p.i., and virus titers were calculated by standard TCID$_{50}$ assay. Average titers and SDs (error bars) for the three replicates are shown.

analysis of N gene transcripts by RT-qPCR indicated a significant increase in the virus titer between 24 and 72 h after virus administration (Fig. 9B). These results indicate that oncolytic efficacy of IRES-controlled viruses depends on intratumoral virus propagation and spread and tumor destruction. This study therefore confirmed that the neuroattenuated IRES-controlled VSVs did retain their oncolytic efficacy.

DISCUSSION

Vesicular stomatitis virus has a wide host range and is able to infect both vertebrate and insect cells (38). VSV has been shown to have superior oncolytic activity against a wide range of cancer cell lines compared to other viruses. Currently, preclinical studies are being carried out with the aim of translating VSV oncolytic virotherapy to the clinic. Although a phase I clinical trial for intratumoral administration of VSV has been recently approved for patients with hepatocellular carcinoma (http://clinicaltrials.gov/show/NCT01628640), neurotoxicity concerns slow the progress of the clinical translation of VSV oncolytic virotherapy for many malignant tumors. Therefore, it is clear that alleviating the neurotoxicity of vesicular stomatitis virus is highly important. Retargeting by modification of the viral glycoprotein, either by direct engineering or by pseudotyping, reduces the efficiency of VSV entry and may therefore reduce the oncolytic potency of the virus (18, 19). The recently developed approach of microRNA targeting has so far led to only small reductions in neurotoxicity (16), and matrix protein mutations that prevent the virus from suppressing innate immune responses are associated with significant reductions in oncolytic potency, particularly in interferon-responsive cancer cells. Therefore, in this study, we attempted to alter viral mRNA translation in a tissue-specific manner without weakening its replication potential.

Earlier workers demonstrated that requirements for *trans*-acting factors differ between related picornavirus IRES elements and can account for cell type-specific differences in IRES function (23, 24). Merrill et al. (27) attenuated poliovirus neurovirulence by switching its IRES element for that of human rhinovirus type 2. A suggested mechanism was that the double-stranded RNA-binding protein 76 (DRBP76) heterodimerizes with nuclear factor of activated T cells (NF45) only in neuronal cells and this heterodimer selectively blocks HRV2 IRES-driven translation initiation in these cells. In another study, the neurovirulence of Theiler's murine encephalomyelitis virus (TMEV) was completely attenuated by replacing its IRES with that of foot-and-mouth disease virus (FMDV) (36). Both the TMEV and FMDV IRESs require eIF2, eIF3, eIF4A, eIF4B, eIF4F, and the pyrimidine tract-binding protein (PTB) for translation initiation, but the FMDV IRES additionally requires the IRES-specific cellular *trans*-acting factor 45

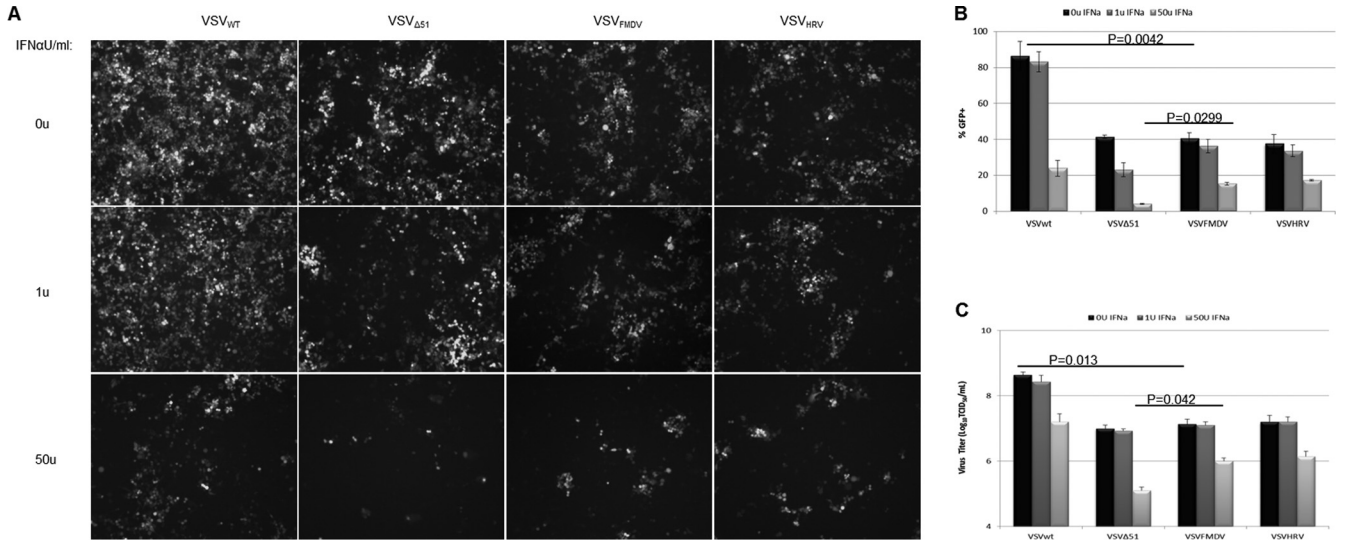

FIG 6 Determination of immune evasion properties of IRES-controlled viruses. After treatment with various concentrations of IFN-α for 24 h, VSV replication and viral protein expression levels were examined. (A) Replication of VSVs was determined by fluorescence microscopy. (B) GFP-expressing cells from the panel A were quantified using ImageJ software (means of three areas are shown). (C) Viral titers were determined by standard $TCID_{50}$ assay. Average titers and SDs (error bars) for the three replicates are shown.

($ITAF_{45}$), a proliferation-dependent protein that is not expressed in murine brain cells (36).

In the current study, we engineered IRES elements of FMDV and HRV2 into an oncolytic VSV in an effort to control its lethal neurotoxicity. Since the matrix protein plays a major role in viral cytotoxicity and immune evasion, we opted to control the expression of the M gene by engineering IRES elements into the VSV genome. In this approach, the IRES elements were inserted before

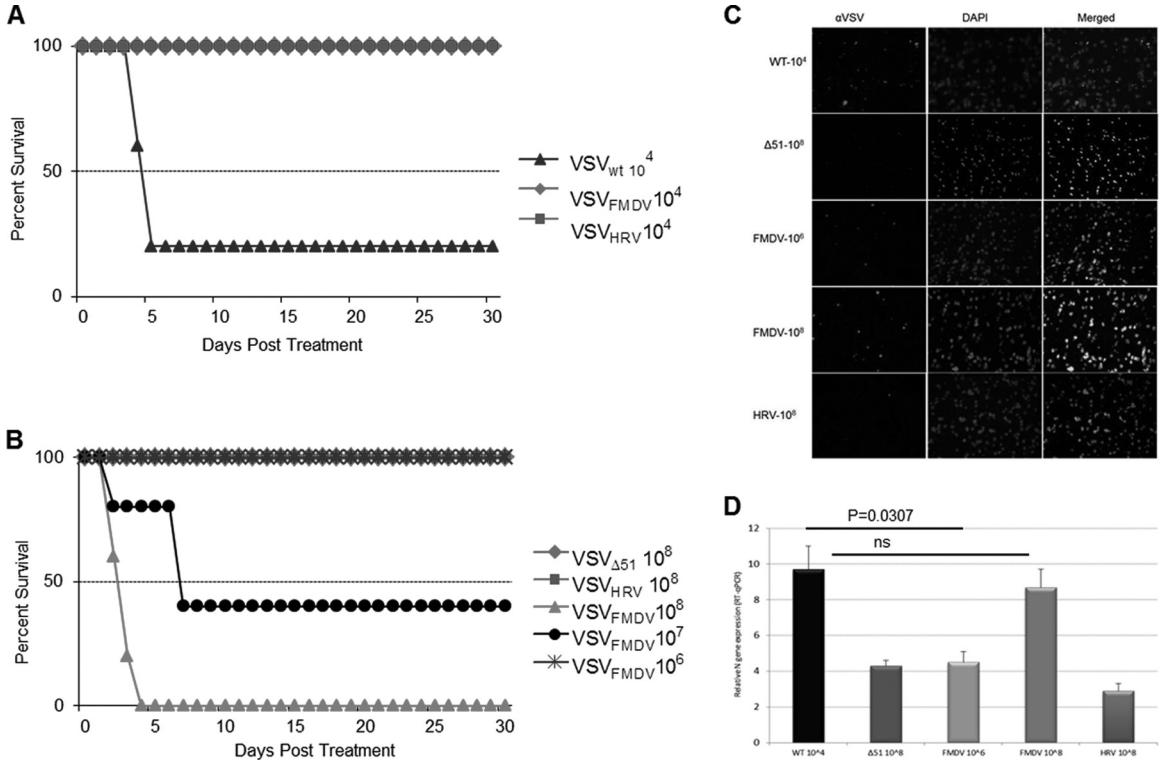

FIG 7 Attenuation of VSV neurovirulence by IRES elements. (A and B) Kaplan-Meier survival graphs for mice (BALB/c, 4 weeks old) inoculated intracranially with 1×10^4 $TCID_{50}$s (A) and 1×10^6 to 10^8 $TCID_{50}$s (B) of rVSV particles and monitored for signs of neurotoxicity. (C) VSV-injected (intracranially) mouse brain was harvested at 48 h p.i., frozen in OCT, and sectioned, and immunofluorescence staining was performed to detect VSV (red) and nuclei (blue). (D) Relative expression of the N gene in the indicated mouse brain by real-time PCR analysis. The data are the N gene level normalized to the GAPDH RNA level relative to that in brain tissue and are represented as mean ± SDs ($n = 3$).

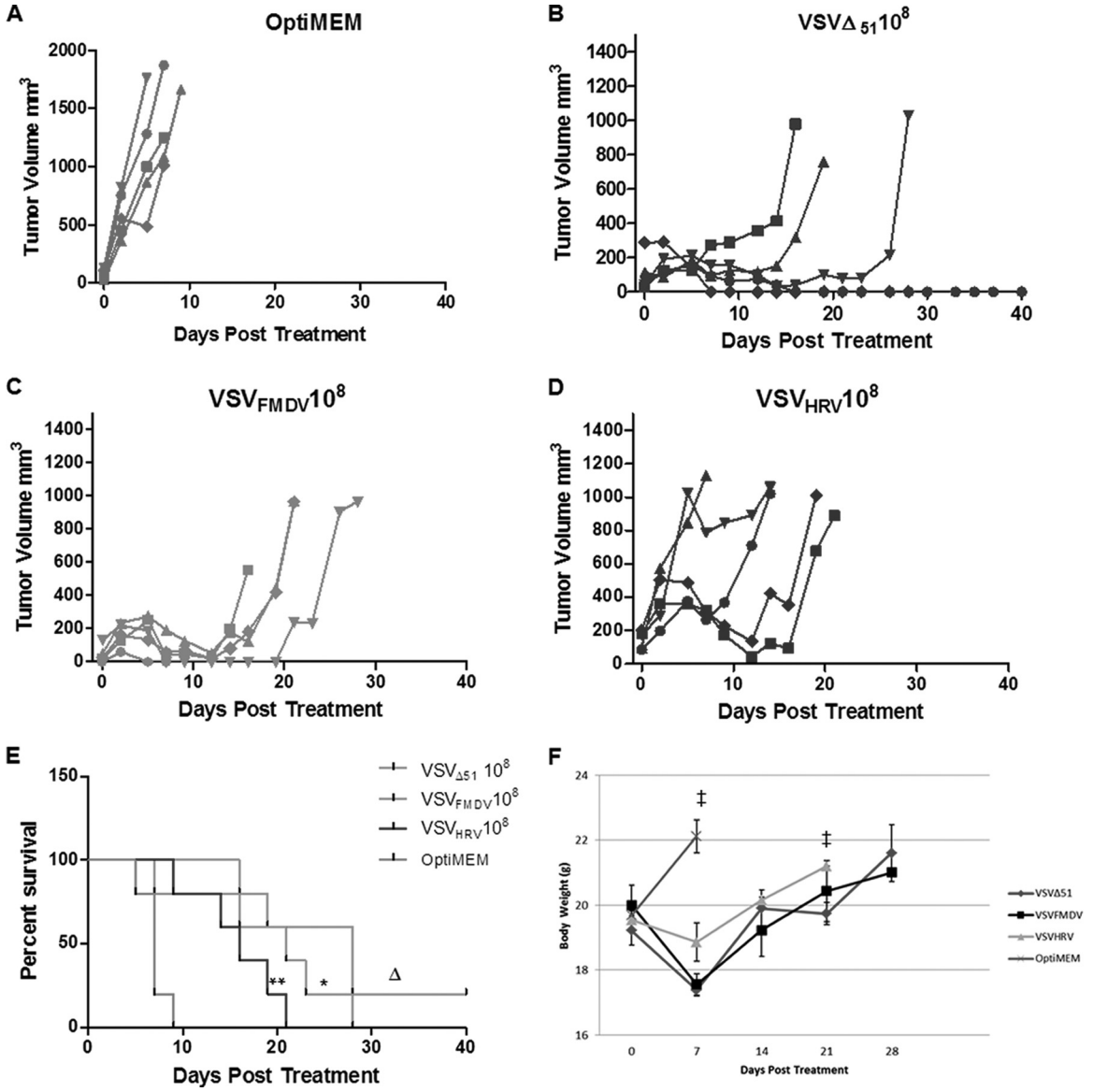

FIG 8 Oncolytic efficacy of IRES-controlled viruses. (A to D) Mice (BALB/c, 4 weeks old) bearing subcutaneous MPC-11 tumors were treated with a single intravenous dose (1×10^8) of Opti-MEM (A), $VSV_{\Delta 51}$ (B), VSV_{FMDV} (C), or (D) VSV_{HRV}. Tumor size was measured by serial caliper measurements. (E) Kaplan-Meier survival curves for the mice from panels A through D. *, $P = 0.0009$ versus Opti-MEM; **, $P = 0.0052$ versus Opti-MEM; Δ, $P = 0.2263$ versus VSV_{FMDV}, $P = 0.0466$ versus VSV_{HRV}, and $P = 0.1883$ VSV_{FMDV} versus VSV_{HRV}. (F) Mouse body weight analysis. The average body weight per group throughout the experiment is plotted as the mean ± SD. ‡, no mouse was left after this point.

the start codon of the M gene, leading to the successful recovery of IRES-controlled VSVs. During negative-sense RNA virus transcription, the polymerase enters the genome exclusively at the 3′ genomic promoter, initiates RNA synthesis, and terminates prematurely at gene junctions, which leads to a transcriptional gradient across the genome from N to L (39, 40). While it is unlikely that IRES insertion would cause disruption to the transcriptional gradient, attenuated translation of the downstream gene may cause significant disruption of the corresponding protein gradient when the particular gene is put under the control of the IRES. This was confirmed by the quantitative analysis of viral proteins and transcripts (Fig. 2 and 3).

Vesicular stomatitis virus is known for its high susceptibility to host innate immunity. To compare the abilities of IRES-controlled versus wild-type or matrix-mutated (ΔM51) VSVs to combat innate immunity, we infected alpha interferon-pretreated HeLa cells with the recombinant viruses. After 24 h of pretreatment with IFN-α, the replication of all viruses was restricted to some extent, resulting in at least a 1-log reduction in viral titers. Even though the level of M gene translation was low, the growth pattern of the IRES-controlled viruses was similar to that of VSV_{wt}, indicating that the IRES-controlled viruses can still partially counteract the cellular antiviral state. In contrast, the replication of the VSV M mutant ($VSV_{\Delta 51}$) was severely restricted due to its inability to turn off host gene expression.

Although primary neurons were not completely resistant to the

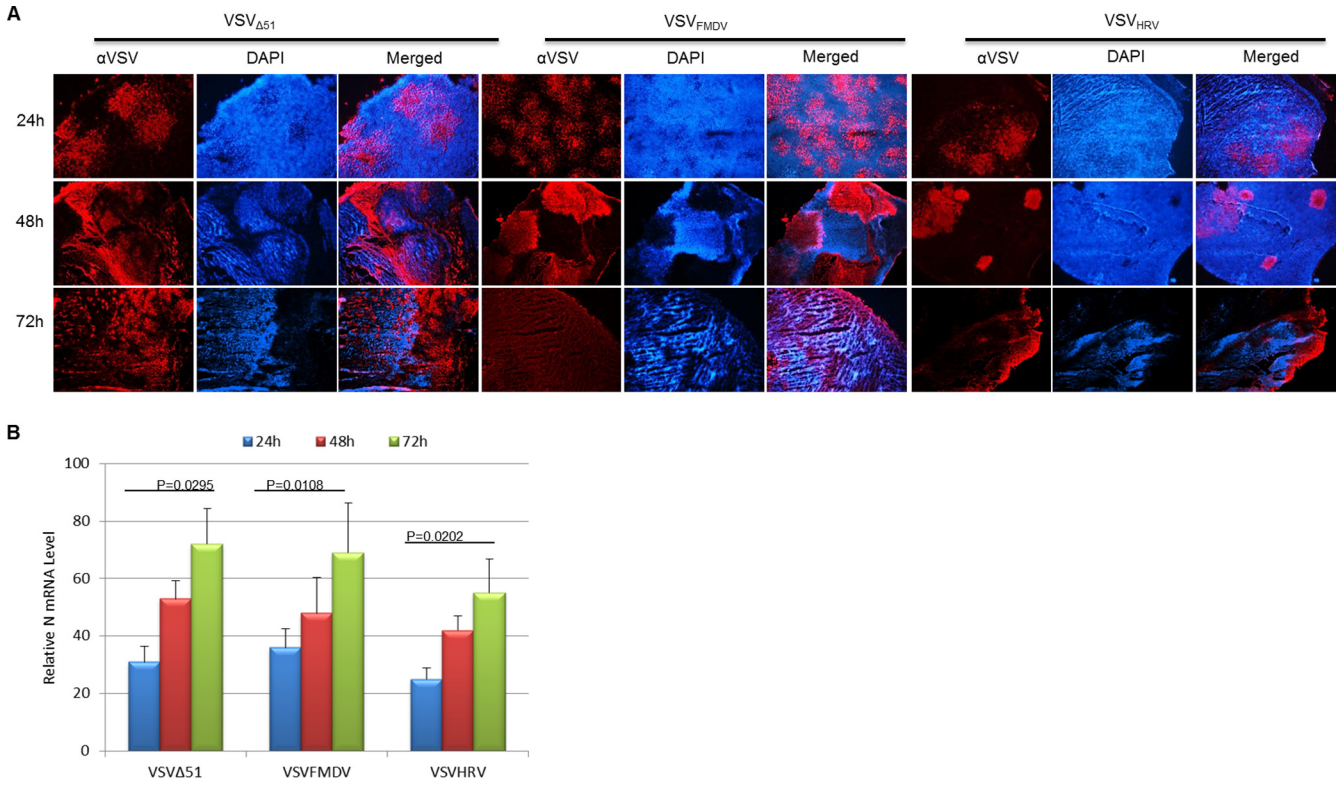

FIG 9 Analysis of virus spread in myeloma tumors *in vivo*. (A) MPC-11 tumor-bearing mice were injected with a single intravenous dose (10^8 $TCID_{50}$s) of the indicated viruses. Tumors were harvested and sectioned at 24, 48, and 72 h posttreatment and immunohistochemistry (IHC) carried out to detect VSV antigen (red) and cell nuclei (Hoechst/blue). Magnification, ×40. (B) Relative expression of the N gene in the indicated mouse tumor by real-time PCR analysis. The data are the N gene level normalized to the GAPDH RNA level relative to that in tumor tissue and are represented by the mean ± SD ($n = 3$).

IRES-controlled viruses *in vitro*, animal studies revealed a high degree of protection against lethal encephalitis, as observed earlier for rabies virus (30). At the dose level of 10^4 $TCID_{50}$s, wild-type VSV administered intracranially killed 80% of immunocompetent mice, while the IRES-controlled viruses did not cause any morbidity or mortality. When higher doses were explored, we found out that VSV_{FMDV} can cause lethal encephalitis only at 10^7 $TCID_{50}$s, and even at this dose, 40% of mice survived without any symptoms. Interestingly, VSV_{HRV} caused no morbidity or mortality even at the highest does level (10^8 $TCID_{50s}$). These toxicity studies explicitly demonstrate that neurovirulence of VSV could be effectively controlled by picornaviral IRES elements. The major rationale behind this study was to translate VSV into the clinic as a cancer therapy. We therefore examined the oncolytic potential of the IRES-controlled viruses *in vivo*. Both VSV_{FMDV} and VSV_{HRV} effectively suppressed the growth of MPC-11 plasmacytomas in immunocompetent mice and prolonged the survival time significantly. The oncolytic efficacy of VSV_{HRV} was lower than that of VSV_{FMDV}, which may be attributed to its slower growth kinetics.

Several methods have been previously developed for attenuation of VSV neurovirulence: M gene mutation (9), G gene deletion (41), microRNA targeting (16), and pseudotyping (18, 19). Each method has its own advantages and disadvantages. In the case of M mutant virus (VSVΔ51), matrix protein was attenuated to eliminate the neurotoxicity of VSV. This virus has proven to be an effective oncolytic agent in many preclinical studies (1, 42–44) but has significantly reduced potency compared to that of wild-type VSV (45, 46). The tumors which have full or partial antiviral signaling pathways are highly resistant to oncolytic VSV infection. Therefore, it is necessary to use other agents (47) or drugs (48, 49) to enhance the viral replication and spread inside the tumor. This current method utilizes wild-type matrix protein, which can counteract the host antiviral response significantly compared to M mutant virus. This results in better replication and higher oncolytic efficacy in interferon-responsive tumors. microRNA targeting is one effective means of restricting viral replication in specific tissues. microRNA has been successfully used to attenuate the pathogenicity of many viruses (50–53). Our earlier attempt to restrict VSV replication in neurons resulted in little success (16). The major concern with this strategy is generation of a spontaneous mutation which results in loss of function of microRNA targets. On the other hand, since our current strategy uses IRES-dependent translation, any mutation will result in viral inactivation, which forces the virus to maintain the inserted structures without any alteration.

It has been demonstrated that VSV has efficiently killed many cancer cells, i.e., osteosarcoma (54), primary adult T-cell leukemia (55), and pancreatic adenocarcinoma (56) cells, in time- and dose-dependent manners. Therefore, it is of paramount importance to produce high-titer virus for clinical translation (57). Since pseudotyped (17–19) and replication-incompetent (19) viruses cannot easily be manufactured, clinical translation of these viruses will be a difficult task. The IRES-controlled VSVs therefore have

potential advantages over other pseudotyped viruses in that they can be produced at very high titers and there is a lower risk of reversion to virulence. Overall, our data provide an important proof of concept that picornavirus IRES-controlled gene expression can ameliorate the development of VSV encephalitis, even when the virus is administered intracranially. A further study will be carried out to investigate the impact of IRES positioning upstream of other genes in the VSV genome. An animal model will be developed to test the efficacy of IRES-controlled VSVs in interferon-responsive tumors. At the same time, more efforts will be undertaken to enhance the oncolytic efficacy of VSV. Most importantly, we have shown that IRES-controlled VSVs have an increased therapeutic index due to a better safety profile without compromise to their oncolytic efficacy.

REFERENCES

1. **Alajez NM, Mocanu JD, Shi W, Chia MC, Breitbach CJ, Hui AB, Knowles S, Bell JC, Busson P, Takada K, Lo KW, O'Sullivan B, Gullane P, Liu FF.** 2008. Efficacy of systemically administered mutant vesicular stomatitis virus (VSVDelta51) combined with radiation for nasopharyngeal carcinoma. Clin. Cancer Res. **14**:4891–4897.
2. **Naik S, Nace R, Federspiel MJ, Barber GN, Peng KW, Russell SJ.** 2012. Curative one-shot systemic virotherapy in murine myeloma. Leukemia **26**:1870–1878.
3. **Shinozaki K, Ebert O, Woo SL.** 2005. Treatment of multi-focal colorectal carcinoma metastatic to the liver of immune-competent and syngeneic rats by hepatic artery infusion of oncolytic vesicular stomatitis virus. Int. J. Cancer **114**:659–664.
4. **Stojdl DF, Lichty B, Knowles S, Marius R, Atkins H, Sonenberg N, Bell JC.** 2000. Exploiting tumor-specific defects in the interferon pathway with a previously unknown oncolytic virus. Nat. Med. **6**:821–825.
5. **Willmon CL, Saloura V, Fridlender ZG, Wongthida P, Diaz RM, Thompson J, Kottke T, Federspiel M, Barber G, Albelda SM, Vile RG.** 2009. Expression of IFN-beta enhances both efficacy and safety of oncolytic vesicular stomatitis virus for therapy of mesothelioma. Cancer Res. **69**:7713–7720.
6. **Letchworth GJ, Rodriguez LL, Del cbarrera J.** 1999. Vesicular stomatitis. Vet. J. **157**:239–260.
7. **Newcomb WW, Tobin GJ, McGowan JJ, Brown JC.** 1982. In vitro reassembly of vesicular stomatitis virus skeletons. J. Virol. **41**:1055–1062.
8. **Jayakar HR, Murti KG, Whitt MA.** 2000. Mutations in the PPPY motif of vesicular stomatitis virus matrix protein reduce virus budding by inhibiting a late step in virion release. J. Virol. **74**:9818–9827.
9. **Petersen JM, Her LS, Varvel V, Lund E, Dahlberg JE.** 2000. The matrix protein of vesicular stomatitis virus inhibits nucleocytoplasmic transport when it is in the nucleus and associated with nuclear pore complexes. Mol. Cell. Biol. **20**:8590–8601.
10. **Stojdl DF, Lichty BD, tenOever BR, Paterson JM, Power AT, Knowles S, Marius R, Reynard J, Poliquin L, Atkins H, Brown EG, Durbin RK, Durbin JE, Hiscott J, Bell JC.** 2003. VSV strains with defects in their ability to shutdown innate immunity are potent systemic anti-cancer agents. Cancer Cell **4**:263–275.
11. **Barber GN.** 2004. Vesicular stomatitis virus as an oncolytic vector. Viral Immunol. **17**:516–527.
12. **Rabinowitz SG, Huprikar J, Dal Canto MC.** 1981. Comparative neurovirulence of selected vesicular stomatitis virus temperature-sensitive mutants of complementation groups II and III. Infect. Immun. **33**:120–125.
13. **Reiss CS, Plakhov IV, Komatsu T.** 1998. Viral replication in olfactory receptor neurons and entry into the olfactory bulb and brain. Ann. N. Y. Acad. Sci. **855**:751–761.
14. **Schellekens H, Smiers-de Vreede E, de Reus A, Dijkema R.** 1984. Antiviral activity of interferon in rats and the effect of immune suppression. J. Gen. Virol. **65**:391–396.
15. **Obuchi M, Fernandez M, Barber GN.** 2003. Development of recombinant vesicular stomatitis viruses that exploit defects in host defense to augment specific oncolytic activity. J. Virol. **77**:8843–8856.
16. **Kelly EJ, Nace R, Barber GN, Russell SJ.** 2010. Attenuation of vesicular stomatitis virus encephalitis through microRNA targeting. J. Virol. **84**:1550–1562.
17. **Muik A, Dold C, Geiss Y, Volk A, Werbizki M, Dietrich U, von Laer D.** 2012. Semireplication-competent vesicular stomatitis virus as a novel platform for oncolytic virotherapy. J. Mol. Med. **90**:959–970.
18. **Ayala-Breton C, Barber GN, Russell SJ, Peng KW.** 2012. Retargeting vesicular stomatitis virus using measles virus envelope glycoproteins. Hum. Gene Ther. **23**:484–491.
19. **Muik A, Kneiske I, Werbizki M, Wilflingseder D, Giroglou T, Ebert O, Kraft A, Dietrich U, Zimmer G, Momma S, von Laer D.** 2011. Pseudotyping vesicular stomatitis virus with lymphocytic choriomeningitis virus glycoproteins enhances infectivity for glioma cells and minimizes neurotropism. J. Virol. **85**:5679–5684.
20. **Jang SK, Davies MV, Kaufman RJ, Wimmer E.** 1989. Initiation of protein synthesis by internal entry of ribosomes into the 5′ nontranslated region of encephalomyocarditis virus RNA in vivo. J. Virol. **63**:1651–1660.
21. **Kozak M.** 1989. The scanning model for translation: an update. J. Cell Biol. **108**:229–241.
22. **Kuhn R, Luz N, Beck E.** 1990. Functional analysis of the internal translation initiation site of foot-and-mouth disease virus. J. Virol. **64**:4625–4631.
23. **Pelletier J, Sonenberg N.** 1988. Internal initiation of translation of eukaryotic mRNA directed by a sequence derived from poliovirus RNA. Nature **334**:320–325.
24. **Belsham GJ, Sonenberg N.** 2000. Picornavirus RNA translation: roles for cellular proteins. Trends Microbiol. **8**:330–335.
25. **Lopez-Lastra M, Rivas A, Barria MI.** 2005. Protein synthesis in eukaryotes: the growing biological relevance of cap-independent translation initiation. Biol. Res. **38**:121–146.
26. **Pyronnet S, Pradayrol L, Sonenberg N.** 2000. A cell cycle-dependent internal ribosome entry site. Mol. Cell **5**:607–616.
27. **Merrill MK, Dobrikova EY, Gromeier M.** 2006. Cell-type-specific repression of internal ribosome entry site activity by double-stranded RNA-binding protein 76. J. Virol. **80**:3147–3156.
28. **Gromeier M, Alexander L, Wimmer E.** 1996. Internal ribosomal entry site substitution eliminates neurovirulence in intergeneric poliovirus recombinants. Proc. Natl. Acad. Sci. U. S. A. **93**:2370–2375.
29. **Campbell SA, Mulvey M, Mohr I, Gromeier M.** 2007. Attenuation of herpes simplex virus neurovirulence with picornavirus cis-acting genetic elements. J. Virol. **81**:791–799.
30. **Marschalek A, Finke S, Schwemmle M, Mayer D, Heimrich B, Stitz L, Conzelmann KK.** 2009. Attenuation of rabies virus replication and virulence by picornavirus internal ribosome entry site elements. J. Virol. **83**:1911–1919.
31. **Lawson ND, Stillman EA, Whitt MA, Rose JK.** 1995. Recombinant vesicular stomatitis viruses from DNA. Proc. Natl. Acad. Sci. U. S. A. **92**:4477–4481.
32. **Finney, DJ.** 1964. Statistical methods in biological assay, 2nd ed. Hafner, New York, NY.
33. **Storey DG, Kang CY.** 1985. Vesicular stomatitis virus-infected cells fuse when the intracellular pool of functional M protein is reduced in the presence of G protein. J. Virol. **53**:374–383.
34. **Takehara M.** 1975. Polykaryocytosis induced by vesicular stomatitis virus infection in BHK-21 cells. Arch. Virol. **49**:297–306.
35. **Ahmed M, Cramer SD, Lyles DS.** 2004. Sensitivity of prostate tumors to wild type and M protein mutant vesicular stomatitis viruses. Virology **330**:34–49.
36. **Pilipenko EV, Pestova TV, Kolupaeva VG, Khitrina EV, Poperechnaya AN, Agol VI, Hellen CU.** 2000. A cell cycle-dependent protein serves as a template-specific translation initiation factor. Genes Dev. **14**:2028–2045.
37. **Faul EJ, Lyles DS, Schnell MJ.** 2009. Interferon response and viral evasion by members of the family rhabdoviridae. Viruses **1**:832–851.
38. **Albertini AA, Baquero E, Ferlin A, Gaudin Y.** 2012. Molecular and cellular aspects of rhabdovirus entry. Viruses **4**:117–139.
39. **Fearns R, Collins PL.** 1999. Role of the M2-1 transcription antitermination protein of respiratory syncytial virus in sequential transcription. J. Virol. **73**:5852–5864.
40. **Iverson LE, Rose JK.** 1981. Localized attenuation and discontinuous synthesis during vesicular stomatitis virus transcription. Cell **23**:477–484.
41. **Duntsch CD, Zhou Q, Jayakar HR, Weimar JD, Robertson JH, Pfeffer LM, Wang L, Xiang Z, Whitt MA.** 2004. Recombinant vesicular stomatitis virus vectors as oncolytic agents in the treatment of high-grade gliomas in an organotypic brain tissue slice-glioma coculture model. J. Neurosurg. **100**:1049–1059.
42. **Goel A, Carlson SK, Classic KL, Greiner S, Naik S, Power AT, Bell JC, Russell SJ.** 2007. Radioiodide imaging and radiovirotherapy of multiple

myeloma using VSV(Delta51)-NIS, an attenuated vesicular stomatitis virus encoding the sodium iodide symporter gene. Blood **110**:2342–2350.
43. **Hadaschik BA, Zhang K, So AI, Fazli L, Jia W, Bell JC, Gleave ME, Rennie PS.** 2008. Oncolytic vesicular stomatitis viruses are potent agents for intravesical treatment of high-risk bladder cancer. Cancer Res. **68**: 4506–4510.
44. **Lichty BD, Stojdl DF, Taylor RA, Miller L, Frenkel I, Atkins H, Bell JC.** 2004. Vesicular stomatitis virus: a potential therapeutic virus for the treatment of hematologic malignancy. Hum. Gene Ther. **15**:821–831.
45. **Ebert O, Harbaran S, Shinozaki K, Woo SL.** 2005. Systemic therapy of experimental breast cancer metastases by mutant vesicular stomatitis virus in immune-competent mice. Cancer Gene Ther. **12**:350–358.
46. **Wu L, Huang TG, Meseck M, Altomonte J, Ebert O, Shinozaki K, Garcia-Sastre A, Fallon J, Mandeli J, Woo SL.** 2008. rVSV(M Delta 51)-M3 is an effective and safe oncolytic virus for cancer therapy. Hum. Gene Ther. **19**:635–647.
47. **Paglino JC, van den Pol AN.** 2011. Vesicular stomatitis virus has extensive oncolytic activity against human sarcomas: rare resistance is overcome by blocking interferon pathways. J. Virol. **85**:9346–9358.
48. **Alain T, Lun X, Martineau Y, Sean P, Pulendran B, Petroulakis E, Zemp FJ, Lemay CG, Roy D, Bell JC, Thomas G, Kozma SC, Forsyth PA, Costa-Mattioli M, Sonenberg N.** 2010. Vesicular stomatitis virus oncolysis is potentiated by impairing mTORC1-dependent type I IFN production. Proc. Natl. Acad. Sci. U. S. A. **107**:1576–1581.
49. **Diallo JS, Le Boeuf F, Lai F, Cox J, Vaha-Koskela M, Abdelbary H, MacTavish H, Waite K, Falls T, Wang J, Brown R, Blanchard JE, Brown ED, Kirn DH, Hiscott J, Atkins H, Lichty BD, Bell JC.** 2010. A high-throughput pharmacoviral approach identifies novel oncolytic virus sensitizers. Mol. Ther. **18**:1123–1129.
50. **Cawood R, Chen HH, Carroll F, Bazan-Peregrino M, van Rooijen N, Seymour LW.** 2009. Use of tissue-specific microRNA to control pathology of wild-type adenovirus without attenuation of its ability to kill cancer cells. PLoS Pathog. **5**:e1000440. doi:10.1371/journal.ppat.1000440.
51. **Edge RE, Falls TJ, Brown CW, Lichty BD, Atkins H, Bell JC.** 2008. A let-7 MicroRNA-sensitive vesicular stomatitis virus demonstrates tumor-specific replication. Mol. Ther. **16**:1437–1443.
52. **Kelly EJ, Hadac EM, Greiner S, Russell SJ.** 2008. Engineering microRNA responsiveness to decrease virus pathogenicity. Nat. Med. **14**:1278–1283.
53. **Ylosmaki E, Hakkarainen T, Hemminki A, Visakorpi T, Andino R, Saksela K.** 2008. Generation of a conditionally replicating adenovirus based on targeted destruction of E1A mRNA by a cell type-specific MicroRNA. J. Virol. **82**:11009–11015.
54. **Kubo T, Shimose S, Matsuo T, Fujimori J, Sakaguchi T, Yamaki M, Shinozaki K, Woo SL, Ochi M.** 2011. Oncolytic vesicular stomatitis virus administered by isolated limb perfusion suppresses osteosarcoma growth. J. Orthop. Res. **29**:795–800.
55. **Cesaire R, Oliere S, Sharif-Askari E, Loignon M, Lezin A, Olindo S, Panelatti G, Kazanji M, Aloyz R, Panasci L, Bell JC, Hiscott J.** 2006. Oncolytic activity of vesicular stomatitis virus in primary adult T-cell leukemia. Oncogene **25**:349–358.
56. **Murphy AM, Besmer DM, Moerdyk-Schauwecker M, Moestl N, Ornelles DA, Mukherjee P, Grdzelishvili VZ.** 2012. Vesicular stomatitis virus as an oncolytic agent against pancreatic ductal adenocarcinoma. J. Virol. **86**:3073–3087.
57. **Ausubel LJ, Meseck M, Derecho I, Lopez P, Knoblauch C, McMahon R, Anderson J, Dunphy N, Quezada V, Khan R, Huang P, Dang W, Luo M, Hsu D, Woo SL, Couture L.** 2011. Current good manufacturing practice production of an oncolytic recombinant vesicular stomatitis viral vector for cancer treatment. Hum. Gene Ther. **22**:489–497.